PHYSICAL REVIEW E, VOLUME 64, 050802(R)

Surface-tethered chains entangled in a polymer melt: Effects on adhesion dynamics

Scott W. Sides, Gary S. Grest, and Mark J. Stevens
Sandia National Laboratories, Albuquerque, New Mexico 87185-1411
(Received 16 April 2001; published 25 October 2001)

The adhesion between a polymer melt and substrate is studied in the presence of chemically attached chains on the substrate surface. Extensive molecular dynamics simulations have been carried out to study the effect of temperature, tethered chain density (Σ), tethered chain length (N_t), and tensile pull velocity (v) on the adhesive failure mechanisms of pullout and/or scission of the tethered chains. We observe a crossover from pure chain pullout to chain scission as N_t is increased. The value of N_t for which this crossover begins approaches the bulk entanglement length N_e as the temperature is lowered.

DOI: 10.1103/PhysRevE.64.050802 PACS number(s): 61.25.Hq, 61.41.+e, 68.35.Np

Adhesion at polymer interfaces is relevant in either the mixing of two immiscible homopolymers ($A+B$) or attaching a homopolymer melt to a hard surface ($A+$substrate). In both cases, the addition of a third component can increase the entanglements at a polymer interface. For the first case, the extra component is a block copolymer made of the A and B species. For the latter case, the extra component is a layer of the A species that is chemically end-grafted onto the substrate. These tethered polymer layers, or brushes, are relevant in such applications as colloidal stabilization [1,2], filler modification of polymeric materials, and lubrication [3]. Substrate-tethered polymers can also enhance adhesion, i.e., increase the mechanical work needed to break an adhesive bond.

Two key parameters characterizing this system are the length (N_t) and the areal density (Σ) of the tethered chains. Adhesion enhancement due to a tethered polymer layer shows a surprising nonmonotonic behavior as a function of N_t and Σ. The work of adhesion first increases for small values of N_t and Σ in the ''mushroom regime,'' so-called because of the flattened shape of each isolated tethered chain in this regime. Due to the phase behavior of the end-tethered chains in contact with a long polymer melt [4–7], when either N_t or Σ becomes sufficiently large the melt chains are expelled from the tethered chain layer, and the reduced entanglements result in a decrease of the adhesion enhancement. This nonmonotonic behavior for the macroscopic work of adhesion has been observed by Kramer and co-workers in glassy polymers [8–12], and Léger and co-workers in elastomeric materials [7,13].

However, the interplay between the *microscopic* failure mechanisms of tethered chain pullout, scission, and crazing are not fully understood, partly due to the difficulty of direct experimental observation of these phenomena. Molecular dynamics (MD) simulations of fracture in highly crosslinked systems [14,15] and crazing [16–18] have helped to elucidate the crossover from adhesive to cohesive failure of polymer adhesives near walls *without* end-tethered chains. Simulations of tethered chains on small, highly simplified models in two dimensions have been performed [19,20], but were unable to study the effects of chain scission, in particular. In this paper we present large-scale simulations to study the adhesive failure mechanisms of end-tethered chains in contact with an entangled polymer melt.

We perform continuous-space, molecular dynamics simulations on a coarse-grained model of polymer chains. The polymers are represented by attaching spherical beads of mass m with breakable springs. Each nonbonded pair of monomers interacts through a standard (12-6) Lennard-Jones (LJ) interaction $U_{LJ}(r)$, truncated at $r_c=2.2\sigma$, where σ sets the length scale. Bead trajectories are obtained by a stepwise integration of Newton's equations of motion (EOM) using a velocity-Verlet [21] algorithm with a time step $\Delta t=0.006\tau$, where $\tau=\sigma(m/\epsilon)^{1/2}$, with ϵ setting the energy scale. The EOM includes terms for a weak stochastic force and a viscous drag force with a coefficient on the viscous force term of $0.5\tau^{-1}$ [22]. The addition of these two forces to the EOM effectively couples the system to a heat bath.

To study the effect of chain scission on adhesion, the standard finite extensible nonlinear elastic (FENE) potential [22] is altered to allow for broken bonds along a polymer chain. The potential $U_b(r)$, between two adjacent beads a distance r apart on the same chain, takes the form

$$U_b(r)=\begin{cases} U_{LJ}(r)+kr^4[(r-r_1)(r-r_2)]+U_c, & r<r_{br} \\ 0, & r>r_{br} \end{cases}$$

with r_{br} the length at which a bond along the chain is considered broken. The remaining parameters in $U_b(r)$ are $k=-409.12\epsilon/\sigma^6$, $r_1=1.2\sigma$, $r_2=1.219\sigma$, and $U_c=42.059\epsilon$. These parameters come from fitting $U_b(r)$ to the region of the FENE potential near the mean equilibrium bond length, resulting in $r_{br}=1.21\sigma$ and a bond-breaking barrier $\Delta U_b \approx 20\epsilon$. Fitting $U_b(r)$ to a FENE potential this way and using the known radius of gyration from previous simulations, allows construction of initial configurations. The chain-building algorithm used is similar to the one implemented in previous simulations [22]. The form of $U_b(r)$ allows for two extrema in the bond potential; one stable, global minimum near the LJ potential energy minimum, and one local maximum near r_{br} where the bond force becomes zero, allowing bonds to be removed safely from the force calculation without causing large recoil velocities on the resulting chain ends.

To avoid the difficulties in constructing chain configurations for the various wet brush regimes, we restrict the present study to low areal densities Σ in the so-called mushroom regime [4,5]. In this regime each tethered chain inter-

acts weakly with other tethered chains and may be constructed as a Gaussian chain. At higher coverages, the tethered chains begin to phase separate from the melt and it is unclear how to equilibrate these starting configurations within a reasonable amount of computer time. So, for each system of a given N_t and Σ, all chains are constructed as random walks with the correct radius of gyration, and the tethered chains are attached to the substrate wall in random locations. The system size is adjusted so that the tethered chains do not bridge the box, thereby interacting with the other wall. A soft potential is used to remove overlaps and the size of the simulation cell is adjusted until the pressure $P \approx 0$ resulting in an overall monomer density of $\rho \approx 0.85\sigma^{-3}$ ($\rho \approx 0.88\sigma^{-3}$) for the highest (lowest) temperatures used. For all simulations, the number of beads in each of the melt chains is $N_m = 2500$ and the number of tethered chains is $n_t = 30$. The temperatures used range from $T = 1.0\epsilon/k_B$, which is well above the glass transition temperature $T_g = (0.5–0.6)\epsilon/k_B$ [16], down to $T = 0.3\epsilon/k_B$. Simulations are performed using the massively parallel MD code LAMMPS [23], (suitably adapted to include chain scission) developed at Sandia and run on the ASCI Red Teraflop machine and Computational Plant (Cplant) clusters.

Figure 1 shows chain configurations at different times from a tensile pull simulation consisting of approximately 2×10^5 particles with $N_t = 250$. The largest systems contain close to 10^6 particles. The tensile pull is achieved by moving only the bottom wall at constant velocity. The tethered chains are attached to the bottom wall of the simulation cell and the top wall has no chains attached. For speed and simplicity, the wall interaction with the chains is modeled as an integrated LJ potential. The interaction strength of the top wall is set to be sufficiently strong so that no adhesive failure occurs on the top wall during pulling. The interaction of the bottom wall with the melt has a very weak attractive component, so that the adhesion enhancement due to the tethered chains may be studied independently of the adhesion to the bare wall. The z axis is normal to both walls and periodic boundary conditions are used in the x and y directions. The size of the simulation cell in the z direction is set to be approximately three times the radius of gyration of the tethered chains prior to pulling. The red chains are tethered, blue chains represent the melt and green chains were initially tethered and have since broken. The three snapshots illustrate a failure mechanism for a system near the crossover between pure chain pullout and chain scission.

During a pull simulation we measure the remaining length of the tethered chains and the work done by the bottom wall. Figure 2(a) shows the integrated work over time as a function of time $\mathcal{W}(t)$, at different values of N_t for $T = 0.3\epsilon/k_B$, well below the glass transition. Results for different temperatures are shown in Fig. 2(b). For each tethered chain length, $\mathcal{W}(t)$ is plotted for a sufficiently long time such that the tethered chains have either completely pulled out or each of the attached chains has been broken. The plateau in $\mathcal{W}(t)$ at large t signifies the complete debonding of the pulling surface from the entangled melt. Clearly, surfaces with longer tethered chains require more work to completely pull away from the adjacent polymer melt than do short chains.

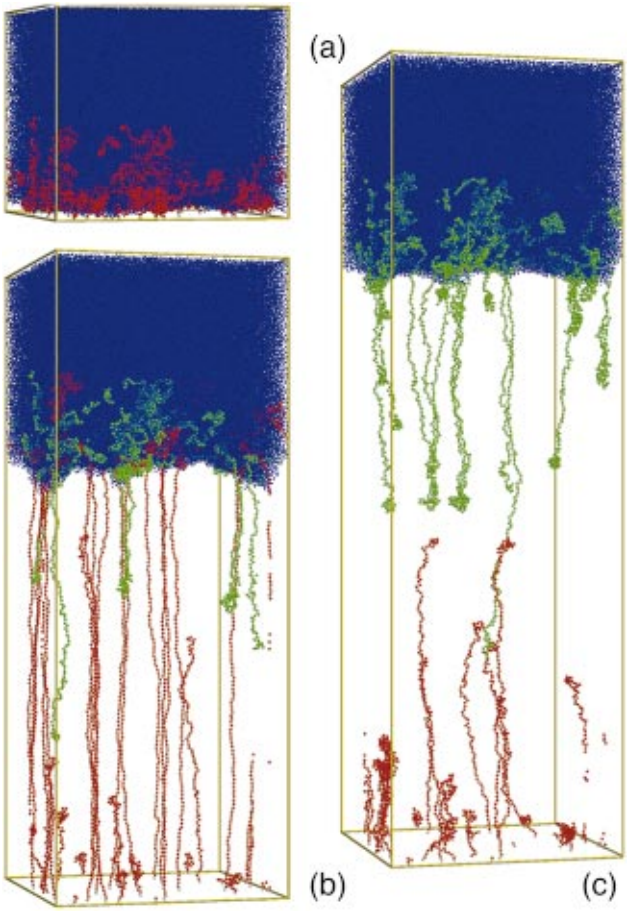

FIG. 1. (Color) Chain configurations at three times during a tensile pull simulation with $T = 1.0\epsilon/k_B$ and pull velocity $v = 0.167\sigma\tau^{-1}$. Elapsed times shown are (a) 60τ, (b) 720τ, and (c) 960τ. The red monomers belong to tethered chains and blue monomers belong to melt chains. Green monomers belong to sections of tethered chains that are no longer attached to the bottom substrate. The tethered chains shown here are for $N_t = 250$ and $\Sigma = 0.008\sigma^{-2}$. Raster3D [24] is used to render the images.

Various theories [20,25] have suggested a power-law dependence for the work of adhesion of the form, N_t^α, where $1 \geqslant \alpha \geqslant 2$. Simulations on simplified models of pullout have suggested that $\alpha = 1$ for small N_t and crosses over to $\alpha = 3/2$ for longer chains. However, the plateau values for $\mathcal{W}(t)$ in Fig. 2(a) do not imply a linear dependence on N_t and tethered chain lengths of $N_t = 250$ and 350 suggest that the amount of work begins to saturate for very long chains. This observation is consistent with the conclusions on the data for chain breaking, presented in Fig. 3 (discussed below). Figure 2(b) shows $\mathcal{W}(t)$, for temperatures below, near, and above T_g. The slope of $\mathcal{W}(t)$ at early and intermediate times is significantly larger for the data at $T \ll T_g$, due to the increased monomeric friction in a glassy state. The total work required to pull the tethered chains from the melt is also larger at low temperatures, as indicated by the plateau values in $\mathcal{W}(t)$ at long times. The large jump in these plateau values is a result of both the increased monomeric friction and a change in the amount of bond breaking in the tethered chains for $T \ll T_g$.

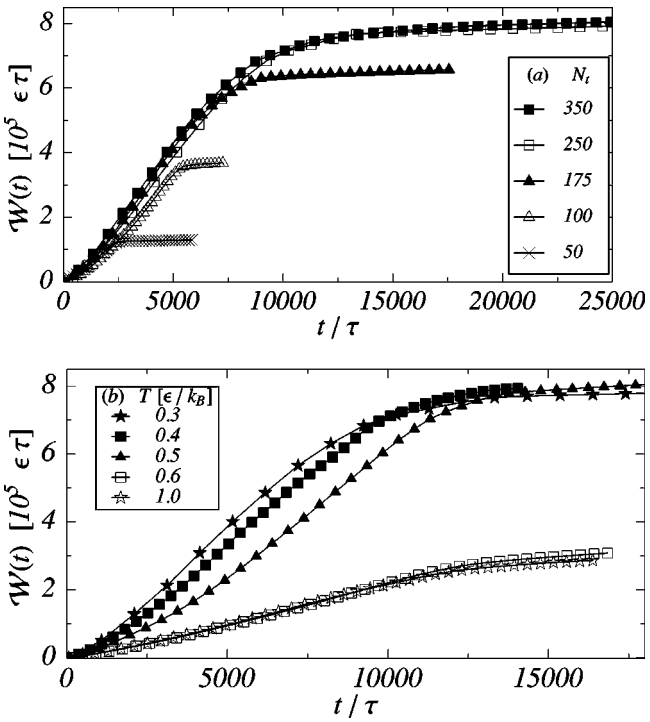

FIG. 2. Total integrated work vs time for (a) different tethered chain lengths N_t for $T=0.3\epsilon/k_B$ and (b) different temperatures for $N_t=250$. All data shown are for $v=0.0167\sigma\tau^{-1}$ and $\Sigma=0.008\sigma^{-2}$.

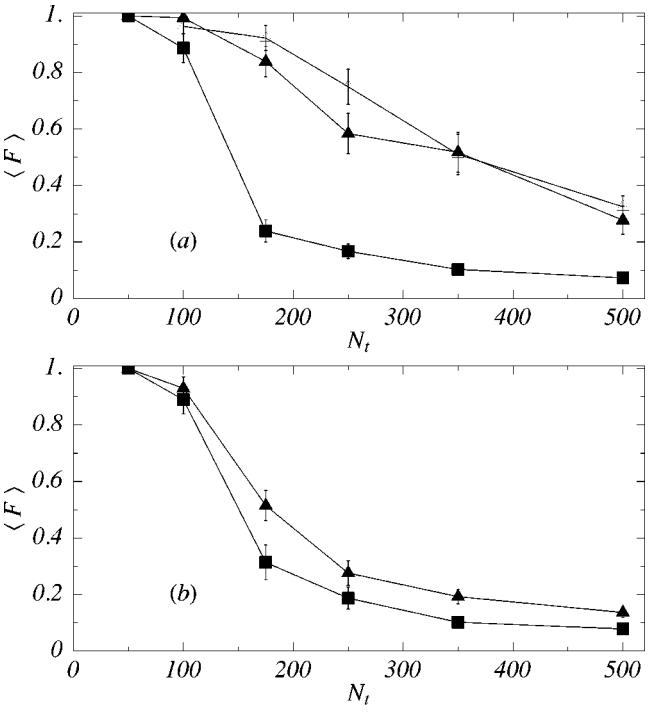

FIG. 3. Average fractional length of remaining tethered chains $\langle F\rangle$ vs initial tethered chain length N_t for (a) $T=1.0\epsilon/k_B$ and (b) $T=0.3\epsilon/k_B$. The symbols denote $v=0.167\sigma\tau^{-1}$, $\Sigma=0.008\sigma^{-2}$ (filled square), $v=0.0167\sigma\tau^{-1}$, $\Sigma=0.008\sigma^{-2}$ (filled triangle), and $v=0.0167\sigma\tau^{-1}$, $\Sigma=0.002\sigma^{-2}$ (open triangle).

The main result of this paper is illustrated in Fig. 3, which shows the average fractional length of remaining tethered chains $\langle F\rangle$ versus N_t. If $N_{t,i}^f$ is defined to be length of the ith tethered chain at the end of a pull simulation, then

$$\langle F\rangle=\frac{1}{n_t}\sum_i^{n_t}\frac{N_{t,i}^f}{N_t},$$

where n_t is the number of tethered chains. The value of $\langle F\rangle$ quantifies the amount of scission in the tethered chains at the end of a pull. $\langle F\rangle=1$ corresponds to pure chain pullout and $\langle F\rangle=0$ to chain scission at the wall for each chain. The filled symbols in Fig. 3 represent data at $\Sigma=0.008\sigma^{-2}$ for two velocities, $v=0.167\sigma\tau^{-1}$ (filled squares) and $v=0.0167\sigma\tau^{-1}$ (filled triangles). Data for two temperatures, $T=1.0\epsilon/k_B$ and $T=0.3\epsilon/k_B$, are shown in Figs. 3(a) and 3(b), respectively. The general trend for all the data is $\langle F\rangle$ decreases as N_t increases, i.e., longer tethered chains tend to break rather than pullout. For $T=1.0\epsilon/k_B$ and $v=0.0167\sigma\tau^{-1}$ the data show an adhesive failure mechanism of almost pure chain pullout for $N_t\lesssim 100$. At $N_t\gtrsim 100$ there is a crossover to a failure mechanism with greater amounts of chain scission as N_t increases. The crossover to chain scission is more dramatic at large v with more chain scission as v is raised. As expected, because the long-chain melt is liquid for $T=1.0\epsilon/k_B>T_g$, bond breaking decreases as v decreases.

However, the crossover to chain scission is nearly independent of v at $T=0.3\epsilon/k_B$, as seen in Fig. 2(b). The beginning of the crossover to chain scission occurs for $50\leqslant N_t\leqslant 100$. The entanglement length calculated from the plateau modulus for this model has been estimated by Pütz *et al.* [26] to be $N_e\approx 72$. This value for N_e is consistent with a value between 50 and 100 for the location of the crossover to chain scission. Therefore, when the tethered chains become sufficiently long to be entangled with the polymer melt they tend to break rather than completely pull out of the melt. As N_t increases well into the chain scission regime, the data approach a $\langle F\rangle\propto 1/N_t$ behavior. Hence, for a given v and T, the amount of chain scission appears to saturate for $N_t\gtrsim 250$, i.e., the average length of the remaining tethered chains approaches a constant value. The open triangles in Fig. 3(a) show data for a smaller areal density of $\Sigma=0.002\sigma^{-2}$. The data in Fig. 3a with $v=0.0167\sigma\tau^{-1}$ for both values of Σ are similar and illustrate that, for these values of Σ, $\langle F\rangle$ is independent of areal density. This confirms our estimates of Σ, which place the system in the mushroom regime.

In conclusion, we performed large-scale MD simulations to study the effects of end-tethered chains on adhesion in a three-dimensional, realistic polymer model. Data is presented that illustrates a crossover from pure chain pullout to increasing chain scission that depends on N_t. For $T<T_g$, the value of N_t near the crossover to scission is consistent with the entanglement length N_e for this model. This result also agrees with experiments on the fracture properties of glassy polymers reinforced by block copolymer additives. These experimental studies report evidence of copolymer scission, as well as a large increase in the work of adhesion,

when the molecular weight of the copolymer increases beyond the entanglement length.

Experimental data also suggest that the large increase in the work of adhesion is due to crazing as the molecular weight of the copolymer increases. The entangled tethered chains presumably transfer enough stress into the melt to initiate crazing. However, crazing is not observed in our simulations even for large N_t and T below the glass transition temperature. The lack of crazing in our simulations could be a result of the simple nature of the tethered chain layer for the mushroom regime. Complex details, such as conformations of the tethered chains as they begin overlap and phase separate for large Σ and N_t, might be crucial to understand crazing. Further work is needed to investigate the effect of tethered chains specifically on crazing mechanisms and the possible roles of chain pullout and scission on craze failure. Work is proceeding to extend simulations to include nonzero bond bending interactions for the coarse-grained model used in this study, as well as applying realistic potentials in explicit-atom models of polymeric materials.

Sandia is a multiprogram laboratory operated by Sandia Corporation, a Lockheed Martin Company, for the U.S. Department of Energy under Contract No. DE-AC04-94AL85000.

[1] D.H. Napper, *Polymeric Stabilization of Colloidal Dispersions* (Academic, London, 1983).
[2] W.B. Russell, D.A. Saville, and W.R. Schowalter, *Colloidal Dispersions* (Cambridge University Press, Cambridge, 1989).
[3] J. Klein, Annu. Rev. Mater. Sci. **26**, 581 (1996).
[4] P.G. deGennes, Macromolecules **13**, 1069 (1980).
[5] M. Aubouy, G.H. Fredrickson, P. Pincus, and E. Raphaël, Macromolecules **28**, 2979 (1995).
[6] G.S. Grest, J. Chem. Phys. **105**, 5532 (1996).
[7] L. Léger, E. Raphaël, and H. Hervet, in *Advances In Polymer Science*, edited by S. Granick (Springer, Berlin, 1999), Vol. 138, p. 185.
[8] C. Creton, E.J. Kramer, and G. Hadziioannou, Macromolecules **24**, 1846 (1991).
[9] J. Washiyama, E.J. Kramer, C.F. Creton, and C.-Y. Hui, Macromolecules **27**, 2019 (1994).
[10] E.J. Kramer, L.J. Norton, C.-A. Dai, Y. Sha, and C.-Y. Hui, Faraday Discuss. **98**, 31 (1994).
[11] L. Norton, V. Smigolova, M. Pralle, A. Hubenko, K. Dai, E. Kramer, S. Hahn, C. Berglund, and B. DeKoven, Macromolecules **28**, 1999 (1995).
[12] C.-A. Dai, E.J. Kramer, J. Washiyama, and C.-Y. Hui, Macromolecules **29**, 7536 (1996).
[13] M. Deruelle, L. Léger, and M. Tirrell, Macromolecules **28**, 7419 (1995).
[14] M.J. Stevens, Macromolecules **34**, 1411 (2001).
[15] M.J. Stevens, Macromolecules **34**, 2710 (2001).
[16] A.R.C. Baljon and M.O. Robbins, Science **271**, 482 (1996).
[17] D. Gersappe and M.O. Robbins, Europhys. Lett. **48**, 150 (1999).
[18] A.R.C. Baljon and M.O. Robbins, Macromolecules **34**, 4200 (2001).
[19] G.T. Pickett, D. Jasnow, and A.C. Balazs, Phys. Rev. Lett. **77**, 671 (1996).
[20] M. Sabouri-Ghomi, S. Ispolatov, and M. Grant, Phys. Rev. E **60**, 4460 (1999).
[21] M. Allen and D. Tildesley, *Computer Simulation of Liquids* (Clarendon, Oxford, 1987).
[22] K. Kremer and G.S. Grest, J. Chem. Phys. **92**, 5057 (1990).
[23] S. Plimpton, J. Comp. Physiol. **117**, 1 (1995).
[24] E.A. Merritt and D.J. Bacon, Methods Enzymol. **277**, 505 (1997).
[25] E. Raphaël and P.G. deGennes, J. Phys. Chem. **96**, 4002 (1992).
[26] M. Pütz, K. Kremer, and G.S. Grest, Europhys. Lett. **49**, 735 (2000), the simulations in this paper used a purely repulsive interaction between nonbonded monomers and a FENE interaction between bonded monomers. The N_e for this model is expected to be very similar to that of the model used in the present study.